Simulation of turbulence mixing in the atmosphere boundary layer and analysis of fractal dimension

IOP Publishing Journal Title
Journal **XX** (XXXX) XXXXXX https://doi.org/XXXX/XXXX

Simulation of turbulence mixing in the atmosphere boundary layer and analysis of fractal dimension

Jackson Tellez-Alvarez[1,3], Konstantin Koshelev[2], Sergei Strijhak[2] and Jose M. Redondo[3]

[1] Institute Flumen, Department of Civil and Environmental Engineering, Technical University of Catalonia, Barcelona, Spain.
[2] Ivannikov Institute for System Programming of the RAS, Moscow, Russia
[3] Department of Physics, Technical University of Catalonia, Barcelona, Spain.

E-mail: jackson.david.tellez@upc.edu, koshelevkb@mail.ru, strijhak@yandex.ru, redondo@fa.upc.edu

Received xxxxxx
Accepted for publication xxxxxx
Published xxxxxx

Abstract

In the first part of this paper, a flow model for numerical simulation of turbulent parameters in Atmospheric Boundary Layer (ABL), based on finite volume method and Large-Eddy Simulation is introduced. This model consists of balance equations for mass, momentum and energy (for potential temperature) equations. The Lagrangian dynamic model of Smagorinsky with restriction of size for the coefficient Cs was used for sub grid turbulent viscosity. The second part of this paper is devoted to the numerical aspects of flow model using Proper Orthogonal Decomposition (POD) method. In the final part of this paper, results from numerical studies on flow in ABL for the neutral and stable case and analysis of fractal dimensions are presented. These results constitute important tests for the assessment of the predictive capacity for the stratified flow model in hand. ImaCalc program was used to study the fractal parameter and structure functions. We calculated the maximum value of fractal dimension D selected among all of the velocity intensity and vorticity modules which was a good indicator of flow's complexity. The data of evolution of D(t) in the middle section of the domain of the multifractal spectra along the main downstream axis were also calculated. The reduction in the maximum value of the Fractal Dimension for intermediate velocity and vorticity values is consistent with Laboratory experiments and with wind wane measurements.

Keywords: Computational Fluids Dynamics, Numerical Simulation, Atmospheric Boundary Layer (ABL), Velocity, Vorticity, Stratified Turbulence and Fractal Dimension.

1. Introduction

The Study of dynamics of vortex structures in the Atmospheric Boundary Layer (ABL) using Large-Eddy Simulation has been performed taking into account the influence of stratification of the environment, the friction produced by the surface using a roughness parameter. The rotation of the Earth, the change of thermal fluxes and a gradient of pressure is important for modelling relevant

variations of the weather and climatic system [1-4]. There are also some other tasks as studying physical processes of pollution near the Earth's surface, designing of wind farms and assessment of their overall performance [5-7].

It is known that the small vortex structures, for example, Hairpin Vortices can be created in the turbulent boundary layer [8-9]. A large number of publications are devoted to the description of similar structures. But not so many papers are devoted to the question of studying the dynamics of large vortex structures (Very-Large-Scale Motions) and the impact assessments of buoyancy forces on their stability [10,11].

Some works are devoted to the analysis of coherent structures dynamic [10, 12, 13]. The purpose of this work is the development of a method for calculation of dynamics of large vortex structures using Large-Eddy Simulation and a method of calculation of various modes energy, assessment of their contribution to a total kinetic energy of turbulence.

The results of calculation parameters in the ABL can be used further as initial data for calculation of parameters of the wind farm in realistic ambient.

Many such processes in geophysical hydrodynamics are highly intermittent with spiky measures and no uniformities. For example, distribution of turbulent kinetic energy dissipation rate. These intermittent processes cannot be described totally by typical moment methods. Therefore, a multifractal method is required.

2. Mathematical model

In this work the approach based on Large-Eddy Simulation (LES) using finite volume method for the solution of the main equations reflecting conservation laws was used: the continuity equation (1), momentum equation (2), transport of scalar value - potential temperature equation (3).

The sub grid-scale models are an important part of LES for ABL. The SGS stress tensor was raised from the filtering of the Navier-Stokes equations. The Boussinesq approximation for buoyancy force is included through the separate term in the momentum equation. The final mathematical model included the following equations (1-8).

$$\frac{\partial \bar{u}_j}{\partial x_j} = 0 \tag{1}$$

$$\frac{\partial \bar{u}_i}{\partial t} = -\frac{\partial}{\partial x_j}\left(\bar{u}_j \bar{u}_i\right) - \frac{\partial R_{ij}^D}{\partial x_j} - \frac{\partial \tilde{p}}{\partial x_i} - \left(\frac{\partial \tilde{p}}{\partial x_i}\right)^d + \left(1 - \frac{\bar{\theta}}{\bar{\theta}^0}\right) g_i + \epsilon_{ij} f^c \bar{u}_j \tag{2}$$

$$\frac{\partial \bar{\theta}}{\partial t} = -\frac{\partial}{\partial x_j}\left(\bar{u}_j \bar{\theta}\right) - \frac{\partial R_{\theta j}}{\partial x_j} \tag{3}$$

$$R_{ij}^D = -2\nu^{SGS}\bar{S}_{ij} \tag{4}$$

$$\bar{S}_{ij} = \frac{1}{2}\left(\frac{\partial \bar{u}_i}{\partial x_j} + \frac{\partial \bar{u}_j}{\partial x_i}\right) \tag{5}$$

$$\nu^{SGS} = (C_s\Delta)^2\left(2\bar{S}_{ij}\bar{S}_{ij}\right)^{1/2} \tag{6}$$

$$R_{\theta j} = -\frac{\nu^{SGS}}{Pr_t}\frac{\partial \bar{\theta}}{\partial x_j} \tag{7}$$

$$\frac{\partial R_{ij}^D}{\partial x_j} = -\frac{\partial}{\partial x_j}\left(\nu^{SGS}\frac{\partial \bar{u}_i}{\partial x_j}\right) - \frac{\partial}{\partial x_j}\left[\nu^{SGS}\left(\frac{\partial \bar{u}_j}{\partial x_i} - \frac{2}{3}\frac{\partial \bar{u}_k}{\partial x_k}\delta_{ij}\right)\right] \tag{8}$$

where, $\bar{u}_j$ is the resolved Cartesian velocity field, $\tilde{p}$ is modified pressure variable, which is the density-normalized deviation in resolved-scale static pressure from its time averaged value (in the absence of finite time-averaged vertical gradients of temperature), $R_{ij}^D = R_{ij} - R_{kk}\delta/3$ is the deviatoric part of the sub-grid-scale (SGS) stress tensor and R_{ij} is the SGS stress tensor, R_{kk} is the trace of the stress tensor. $\left(\frac{\partial \tilde{p}}{\partial x_i}\right)^d$ is as partially constant driving pressure gradient term used to achieve a specified mean geostrophic wind, $\bar{\theta}$ is the resolved virtual potential temperature, $\bar{\theta}^0$ is the reference virtual potential temperature, g_i is the gravity vector, ϵ_{ij} - is the alternating symbol, f^c is the Coriolis parameter, and the subscripts 1, 2, and 3 refer to the x-, y-, and z-directions, respectively. $\bar{\theta}^0$ is set to the initial virtual potential temperature below the capping inversion of 300K.

All physical quantities were defined in the centre of a numerical cell. The features of a land topography, the influence of stratification of the environment, rotation of Earth, change of thermal fluxes were considered for calculation of flow's parameters. The large-scale vortex structures were defined by means of integration the filtered equations [14]. The box filter was used for receiving the filtered equations, the small eddies which size did not exceed a step of a numerical grid were modelled by means of a Lagrangian dynamic model of Smagorinsky for sub grid turbulent viscosity - LASI [15, 16]. For restriction of value for the dynamic constant of Smagorinsky Cs that values of size weren't negative in calculation processes, the additional model with restriction of size for Cs value was used.

The approximation of terms in the equations (1-8) was executed with the second order of accuracy on time and space. The obtained equations for communication of velocity, pressure, potential temperature were solved by means of an iterative algorithm PIMPLE. The procedure a predictor-corrector is realized for values of velocity, pressure, potential temperature as it was made in the paper [17]. The obtained system of the algebraic equations were solved by the iterative method of conjugate gradients with a preconditioner for velocity, pressure, potential temperature, stress tensor and parameters for the turbulence model. The total quantity of the calculated physical values (scalar, vector and tensor) depending on the selected turbulence model for

sub grid viscosity can be from 25 to 33. In this regard resources of computing, cluster is required.

The surface shear stress model was calculated using Schumann model [18]. At the surface, the stress tensor components are equal to zero, except values R_13, R_23.

During calculation fields of average and fluctuation values have been obtained (velocity, pressure, potential temperature, sub grid viscosity, stress tensor, a thermal fluxes and others). ABL Solver solver as a part of open source library OpenFOAM 2.4 in the parallel mode was used for final modelling [19].

3. POD method and Apache Spark framework

The Proper Orthogonal Decomposition (POD) method allows obtaining new data on turbulence and coherent structures. We have applied POD algorithm using Apache Spark framework and LAPACK mathematical library. The POD was first introduced by Lumley in the field of Computational Fluid Dynamics [20]. The present-day analysis uses the method of snapshots introduced by Sirovich [21].

The computation of the POD modes using Equation (9) requires solving ÃU eigenvalue problem. The main idea of POD is to represent the solution u(x,t) of the system (1-8) as a sum of basic functions phii((x) (also called modes) multiplied by time coefficients ai(t).

$$\int_0^T R(t_1,t_2)\phi(t_2)\,dt_2 = \lambda\phi(t_1) \qquad (9)$$

The main problem is the calculation of auto-covariance matrix $R(t_1,t_2)$. The snapshot method proposes that auto-covariance matrix $R(t_1,t_2)$, which can be approximated by a summation of snapshots with equation (10):

$$R_{ij} = \frac{1}{M}\sum_{n=1}^{M} x_i^n x_j^n \qquad (10)$$

The snapshots are assumed to be distanced by a time or a special distance greater than the correlation time or distance.

Apache Spark framework allows processing large amounts of data in computer's memory by distributing the load between the compute nodes, ensuring high fault tolerance (Figure 1).

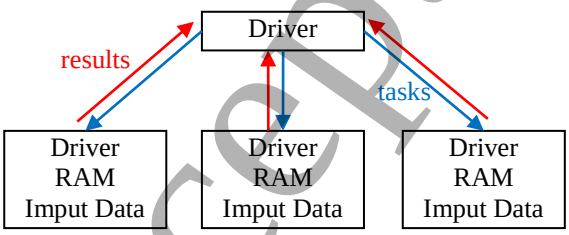

Figure 1. The architecture of Apache Spark framework.

When calculating the flow process, a considerable amount of data in the form of separate time snapshots of the flow was obtained. The utility, written in C++, allowed transferring the data obtained during the hydrodynamic calculation from the OpenFOAM format into the library format, written in Scala. To highlight the characteristic structures, we proposed to use the POD method.

4. Problem definition for GABLS1 case

A series of calculations for turbulent flow for cases in a rectangular area is carried out: 400m x 400m x 400m in stable ABL on various grids are also carried out a comparison with results of these calculations with GABLS1 project [22, 23]. The numerical domain and grid are shown in Figure 2. The logarithmic profile was set as an inlet boundary condition for the value of velocity, for velocity on surfaces the model of function according to the theory of similarity of Monin-Obukhov was used [23, 24].

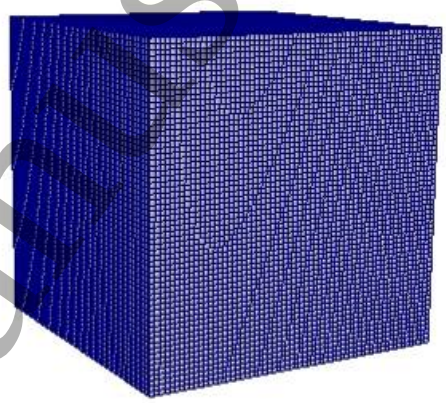

Figure 2. Numerical domain and grid.

The value of potential temperature at the inlet was set to constants up to the certain height and further increased under the linear law. On output borders, the cyclic boundary condition for all physical quantities was set.

The initial parameters for calculation: velocity of wind Ug= (8.0, 0.0, 0.0) m/s; the direction of a velocity vector was of 270 degrees; the value of the rate of surface cooling was 0.25K/h; change of potential temperature with height was from 265K to 269K. The random fluctuations with an amplitude of 0.1K were added on initial values for potential temperature field below 50 m; the surface aerodynamic roughness height was equal to z_0=0.1, the value of heat flux at surface q=7.0x10e-5Km/s, the latitude corresponded to 73 degrees. The density of air was set equal 1.3223kg/m3, and gravity constant g=9.81m/s2. The initial values of a Lagrangian dynamic model of Smagorinsky for sub grid viscosity were equal to LLM=2.56x10e-6m4/s4, LMM=1x10e-4m4/s4. The calculations were performed on two grids: a) 64 x 64 x 64; b) 128 x 128 x 128 cells.

5. Numerical results for GABLS1 case

The data for fields of values (snapshots) with a time step of dT=200 seconds have been obtained during the calculation. There were a total of 150 snapshots. Thus, the physical flow was computed for stable ABL for 30000 seconds. The distribution of value for the instantaneous velocity magnitude at various time points is shown in Figures 3-6. It was observed the changes of U_0 Magnitude values in the course of the calculation.

The correlation matrix for the value of velocity with dimension 146×146 has been created by results of LES. As a result of calculation, it was obtained that 4 first modes contained 95% of the general turbulent energy.

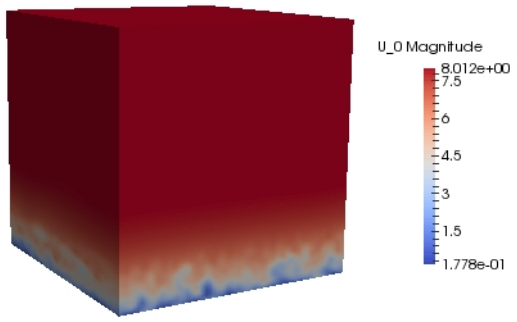

Figure 3. Modulus of the velocity field at t=500 s.

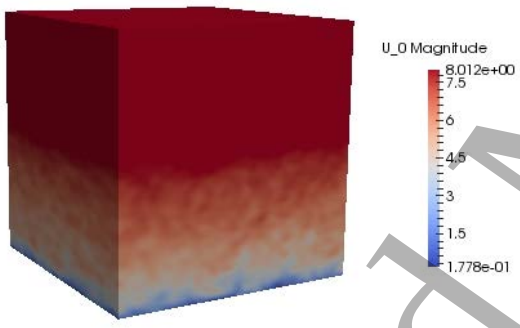

Figure 4. Magnitude velocity field at t=1000 s.

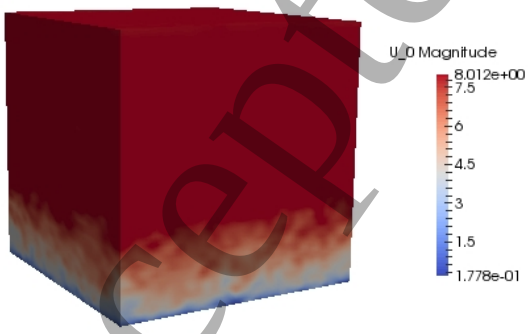

Figure 5. Magnitude velocity field at t=2000 s.

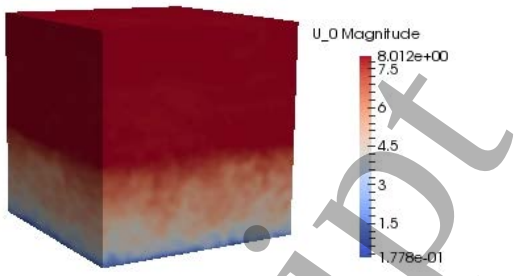

Figure 6. The magnitude of the velocity field at t=3000 s.

The two first modes (basic functions) are shown in Figure 7. In Figure 8, the evolution of the coefficients of the first 4 modes are shown.

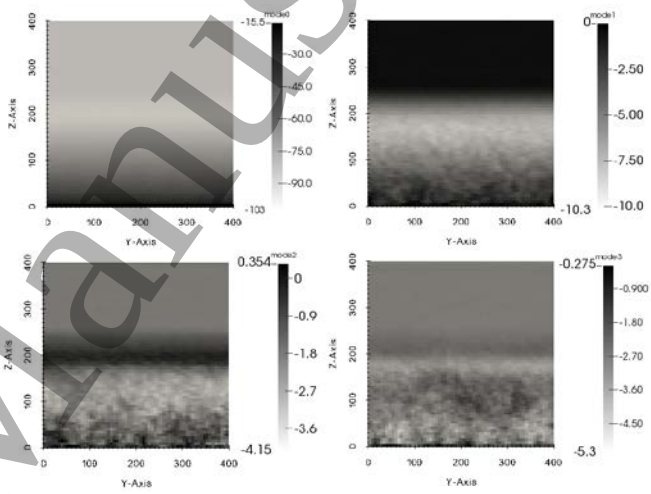

Figure 7. Zero to third modes of x-component for the velocity vector.

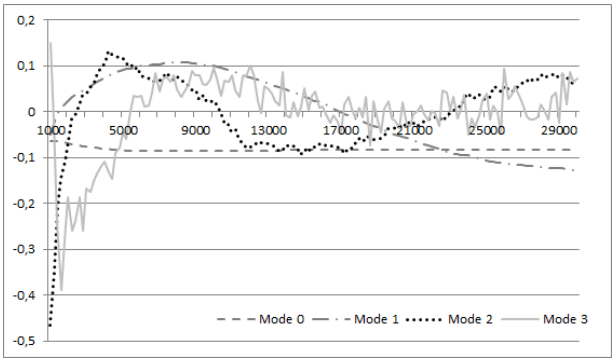

Figure 8. Dependence of temporary coefficients at the first 4 modes from time.

The results of the dependence of velocity and potential temperature from a height, shown in Figures 9 and 10, were in good correlation with results of other simulations in GABLS1 project [22, 23].

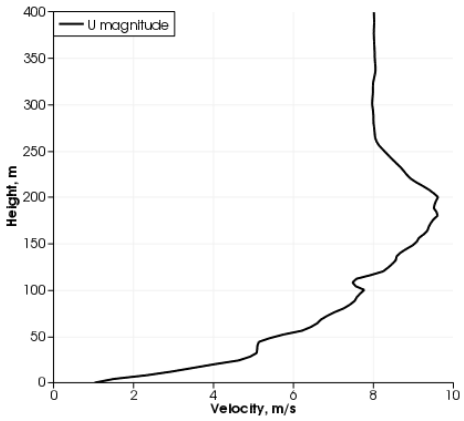

Figure 9. Dependence of horizontal velocity in height.

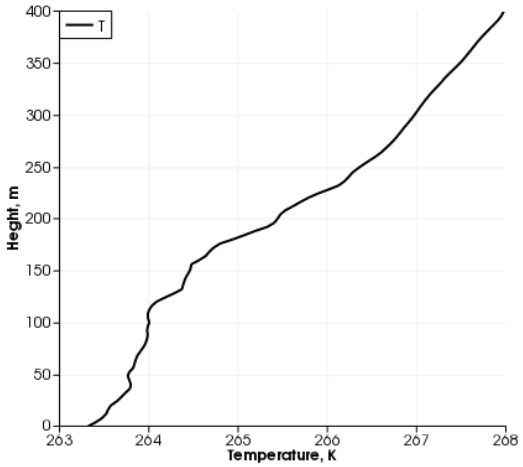

Figure 10. Dependence of potential temperature in height. For the same simulation.

6. Problem definition for a rectangular parallelepiped domain

The spatial area was represented as a rectangular parallelepiped. The boundary condition for the velocity of slipping was used on the upper boundary, and on side borders - a cyclic boundary condition. For the value of velocity on the inlet of numerical domain area the potential profile of velocity was set, for velocity on the surface, the model of wall function according to the theory of similarity of Monin-Obukhov was used. The value of potential temperature on the inlet was set to constants up to the certain height and further increased under the linear law. The surface shear stress model on surfaces was determined by the model of U. Schumann [18]. The initial conditions for a case with neutral ABL were set by the following: wind velocity U0=8m/s with the direction of 270 degrees to which height is set the average velocity of U = 100m, reference potential temperature below 300K and from above 305K, initial value of subnet turbulent kinetic energy of 0.1m2/s2, a gradient of potential temperature of 0.003K/m. Basic parameters for calculation were chosen: molecular number Pr=0.7, turbulent number Prt=0.33, molecular viscosity 1.0e-5 the m2/s, width is 41.3 degrees.

7. Results of simulation for a rectangular parallelepiped case

The calculations were carried out in a spatial area of 3km x 3km x1.02km in size on numerical grids 150 x150x51 and 300x300x102 during 20000 seconds. The numerical domain and grid are shown in Figure 11. Two characteristic options - "neutral" for modelling of a neutral condition of the atmospheric boundary layer (ABL) and "steady" for modelling of a steady condition of ABL are chosen. These options differ in a task of boundary conditions for potential temperature on the Earth's surface. For a case "neutral" the absence of a thermal flux was set. For a "steady" ABL case the thermal flux was calculated taking into account the fixed velocity of cooling of the Earth's surface. Thus, the "steady" case is at the same time a realistic stratified atmospheric wind simulation as shown in figure 10. The considerable stratification of potential temperature in comparison with the "neutral" or un-stratified model. The realistic case shows the maximum vertical density gradient at about 200m, with a maximum Richardson number (Gradient-based) defined as (11):

$$R_i = \frac{-g\frac{\partial \rho}{\partial z}}{\rho\left(\frac{\partial u}{\partial z}\right)^2} \qquad (11)$$

The initial conditions for stable case: wind speed Ug=(8.0, 0.0, 0.0) m/s with direction 2700, the height at which to drive mean wind to U0 was 100 m, initial potential temperature at bottom 300 K, at top 305 K, height of middle of initial inversion 750 m, initial turbulent kinetic energy 0.1 m2 /s2 , potential temperature gradient above inversion 0.003 K/m. The general parameters: molecular Prandtl number 0.7, turbulent Prandtl number, Prt, 0.33, molecular viscosity 1.0E-5 m2/s, the latitude of the Earth 41.3 degree.

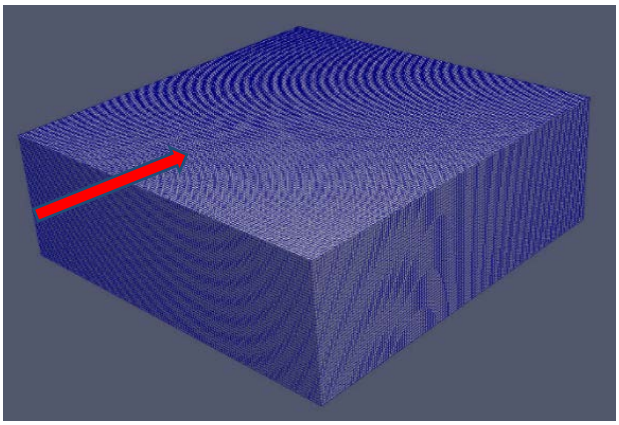

Figure 11. Numerical domain and grid.

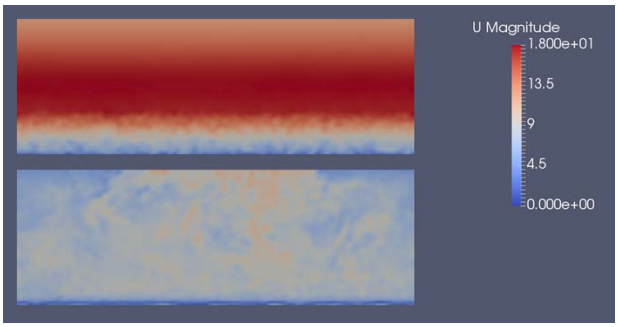

Figure 12. Distribution of an absolute value of velocity. Top – "neutral" non-stratified case, bottom – "stable" stratified realistic case.

The calculated distribution of an absolute value of velocity is given in the central section of the numerical domain in Figure 12. The essential distinction of the behaviour of velocity is visible. For a neutral state, the area of noticeable perturbations is in a limited zone near the Earth's surface while fluctuations for the "steady" case are distributed rather evenly on all area.

The stream wise velocity fluctuations at 90 m above the surface, in the case using numerical mesh 150 x 150 x 51, is shown in Figure 13. These fluctuation values can reach about 25% of the mean velocity value. It is necessary to take these fluctuations of velocity and pressure into account in case of simulations of physical parameters in large wind turbines in wind farms. The mean potential temperature field is shown in Figure 14. So cooling the ground and heating the upper layer produces internal waves dominated by the Brunt-Vaisala frequency (12):

$$N = \left(-\frac{g}{\rho}\frac{\partial \rho}{\partial z}\right)^{1/2} \quad (12)$$

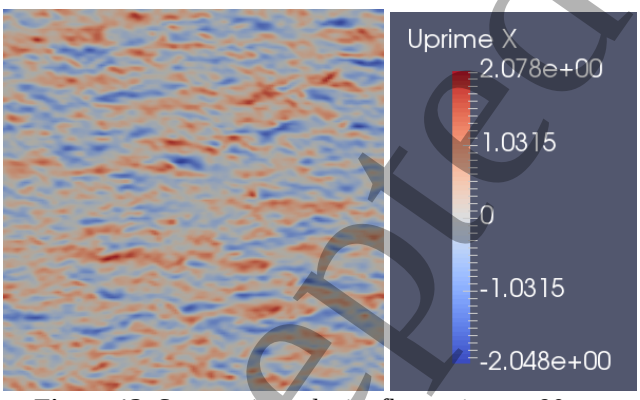

Figure 13. Streamwise velocity fluctuations at 90 m above surface, mesh 150 x 150 x 51

The Q-criterion, lambda2 criterions are often applied for the definition of vorticity in ABL. For the executed calculations the qualitative difference wasn't so big. The distributions of Q-criterion for "neutral" and stratified "steady" options respectively are given in Figure 15. It is seen that absolute values of Q-criterion for a "neutral" case in ABL are more or less of the same size than for a "steady" stratified case in ABL. This difference becomes even more considerable with an increase in height that will quite be coordinated with the evolution and structure of the turbulent flow as Ri(z) from Figures, 9, 10 and 12. As shown by Redondo [25], the fractal and multifractal dimensions are a strong logarithmic function of the local Richardson number.

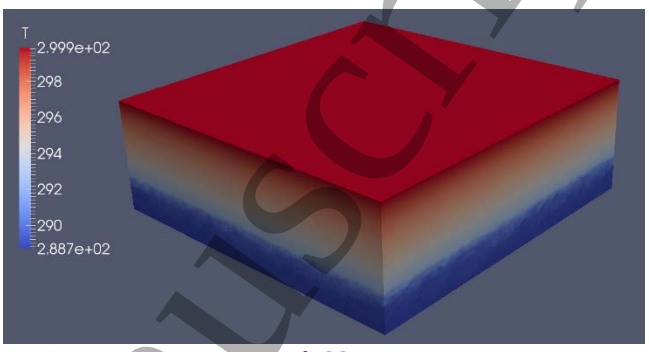

Figure 14. Temperature field

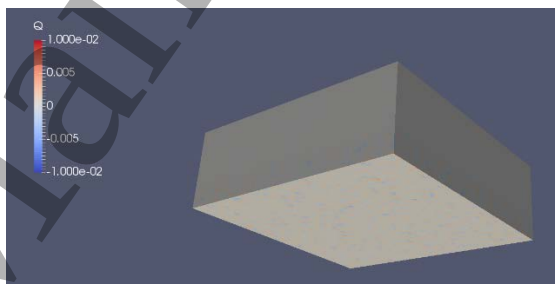

"Neutral" non-stratified ABL

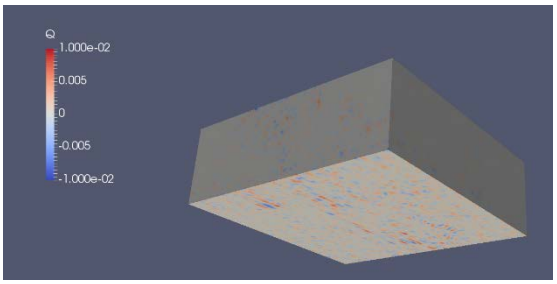

"Steady" stratified ABL

Figure 15. Distributions of Q-criterion.

8 Analysis of Fractal Dimension

In the process of the turbulent eddy three dimensional Kolmogorov type cascade we assume that the basic hypothesis of Kolmogorov [26, 27] apply, namely a) the properties of the eddy hierarchy at a certain scale only depend on the local dissipation at that size ε(L), at scale L and b) that there also exists an intermediate "inertial range" of eddies Lo>> L >>L_k the viscosity does not play any role. In this range, all the properties should be determined by the

stratification acting on the topology of the ABL, L_0 is described as Ozmidov scale and L_k is the smallest turbulent Kolmogorov scale. At least over a range of scales, but keeping a less restrictive homogeneous and locality hypothesis with respect to intermittency), we can relate how the characteristic speed v(L) for eddies of size L depends on L. Since the dimensions of $\varepsilon(L)$ are velocity^2/time, the only dimensional combination of $\varepsilon(L)$ and L yielding a dimensional estimation of (13):

$$v(L) \approx (\varepsilon L)^{1/3} \tag{13}$$

And thus the fractional distribution of the energy per unit mass and length will be (14):

$$E(L)(dL/L) \approx v(L)^2\,(dL/L) \approx (\varepsilon L)^{\frac{2}{3}}(dL/L) \approx \epsilon^{2/3}L^{-1/3}dL \tag{14}$$

That leads to the traditional Kolmogorov spectral 5/3 law (15):

$$E(k)dk \approx \varepsilon^{2/3}k^{-5/3}dk \tag{15}$$

It is also interesting to study the topology of the flow influence of turbulence structure of diffusion, so if we assume that $v(L) \approx L^{1/3}$, with a scaling exponent, the moments of the relative distance R, close to L, between a pair of particles, scale with time as (16):

$$\langle R^{2q}\rangle \approx t^{2q/(1-\ 1)} \tag{16}$$

In the limit of long times. As a consequence, the r.m.s. of the displacement R as a function of time in the long-time limit is given in terms of the first order moment as (17):

$$\langle R^2\rangle \approx t^{2/(1-\zeta_1)} \tag{17}$$

Which is larger than the classical Brownian type of diffusion, and also as suggested by Richardson as early as 1925, with the scaling exponent 1/3 associated with Hurst scaling exponent (18):

$$\langle R^2\rangle \approx t^3 \tag{18}$$

The fact that dissipation is not constant as assumed in the Kolmogorov K41 theory [31] and that it also scales spatially leads to a more general K62 definition of the scaling exponents of the structure functions so that now $\zeta_p = f(h,p)$, is a general function, and not just $\zeta_p = hp = p/3$ (19).

$$\langle v(L)^p\rangle \approx L^{p/3}\langle \varepsilon(L)^{p/3}\rangle \approx L^{\zeta_p} \tag{19}$$

One of the first theories seeking to predict the structure function exponents was in fact given by Kolmogorov in K62 [32], as well as Obukhov, the new intermittency parameter, this parameter has been measured for homogeneous, stationary and isotropic turbulence giving values in the range of 0.2 to 0.6, but for real turbulence, such as in the ABL, the situation seems much more complicated as discussed by Mahjoub [28] (20):

$$\langle \partial\varepsilon(r)\partial\varepsilon(r+L)\rangle \approx \langle \varepsilon^2\rangle (L/L_0)^{-\mu} \tag{20}$$

Thus, the scaling exponents depend both on p, the order, and the intermittency parameter, so the expression for the p^{th} order velocity structure function will be (21):

$$\langle v(L)^p\rangle \approx L^{p/3}L^{\mu p\,(3-p)/18} \tag{21}$$

And the expression for the energy spectra as a function of the wave-number modifies the non-intermittent K41 3D cascade given by the 5/3 law as (22):

$$E(k) \approx \varepsilon^{2/3}k^{-5/3-\mu/9} \tag{22}$$

The general expression for the structure function scaling exponents is then (23):

$$\zeta_p = \frac{p}{3} + \frac{\mu}{18}p(3-p) \tag{23}$$

If we use the relationship between the fractal dimension (or more exactly the maximum of the multifractal measures that described the contours of dissipation (24):

$$L(n) = L_0 2^{-n} \tag{24}$$

And from the fractal dimension definition (25):

$$N(n) = N_0 2^{D_n} \tag{25}$$

The volume at the nth generation of an intermittent vortex cascade is (26):

$$V(n) = N(n)L(n)^3 \approx N_0 L_0^3 2^{-(3-D)n} \tag{26}$$

With a volume ratio of (27):

$$\beta(n) = V(n)/V_0 = 2^{-(3-D)n} = [L(n)/L_0]^{3-D} \tag{27}$$

The lack of dissipation space modifies the traditional definitions of homogenous parameters and further analysis described in Mahjoub et. al. [29] for non-homogeneous turbulence leads to (28-32):

$$\varepsilon \approx \beta(n)v^3(n)\tau^{-1}(n) \tag{28}$$

$$v(n) \approx [\varepsilon L(n)\beta^{-1}(n)]^{1/3} \tag{29}$$

$$E(n) \approx \beta(n)\varepsilon^{2/3}[L(n)/\beta(n)]^{2/3} \tag{30}$$

$$E(k)dk \approx \varepsilon^{2/3}k^{-5/3}[kL_0]^{-(3-D)/3}dk \tag{31}$$

$$\langle v(L)^p\rangle \approx \varepsilon^{p/3}L^{\zeta_p} \tag{32}$$

And thus we obtain what is often called the multifractal method by Frish [30] (33):

$$\zeta_p = \frac{D}{3} + (3 - D)\frac{(3-D)}{3} \quad (33)$$

If we want to estimate diffusion in a fractal environment, we may substitute the first order structure function scaling exponent (D =1) as (34):

$$\zeta_1 = \frac{1}{3} + (3 - 1)\frac{(3-D)}{3} = \frac{1}{3}(7 - 2D) \quad (34)$$

In the models used above, the multifractal dimension should be modified by the changing role of intermittency, which as observed in experiments is affected by buoyancy.

It is worth mentioning that multifractal characteristics do not have a strong effect on diffusion, because it only depends on the scaling law for the first moment of the velocity, which is virtually unchanged by multifractality. More sophisticated data analysis such as the evaluation of integral length scales or local fractal dimensions of the sea surface appearance, together with the detailed information of the position and sizes of the mesoscale dominant eddies or structures of size L or R, provides useful information on the mesoscale turbulence in the ocean and in the atmosphere, after many observations the dominant patterns and the causes of different topological characterizations by Mandelbrot [31], might be understood. It is important to characterize the types and structure of the main vortices detected as well as the spectral cascade processes that take place, these may be investigated by using fractal methods on images of the area [32]. Moreover, previous fractal dimension analysis of the components of the wind velocity was done by Tijerat et al. [38].

According to this theory, the PDFs of the velocity increments present a deviation with regard to the Gaussian, the linear form has been observed [4, 5]; this deviation is the so-called intermittency. Moreover, when there is intermittency, the tails of the PDFs of the velocity increments depart from the Gaussian form and can be approached by stretched exponentials [6-10]. Therefore, the scaling exponents can be used to characterize the turbulence intermittency.

There are many turbulence models that try to explain the phenomenon of the intermittency, for instance, the models corresponding to [11-13]. In [14, 15] several of these methods are explained.

The aim of this article is a new application to atmospheric boundary layer data. In such kind of data, this model is very useful, because can be used in not only conditions of homogeneity and isotropy, as the most of the models.

The physical interpretation of the rate of change of energy scale up to a certain length is equal to the energy injected at a scale by a force minus the energy dissipated at such scales and less the flow of energy at smaller scales. This last term is due to non-linear interactions between the scales derived from the nonlinear term in the Navier-Stokes equation. This non-linear term is responsible for the unpredictable behaviour of turbulent flows. J would express the baroclinic vorticity production with a variation of density with "potential height" i.e. (35)

$$J = \frac{1}{\rho^2}\nabla\rho \times \nabla\rho \quad (35)$$

The evolution of vorticity in time is then (36):

$$\frac{\partial\omega}{\partial t} = J - (u \cdot \nabla)\omega + [(\omega + 2\Omega) \cdot \nabla]u - \nu\nabla^2\omega \quad (36)$$

a) Image of the vorticity field

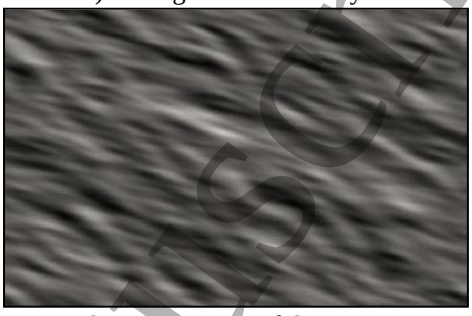

b) Histogram of the image

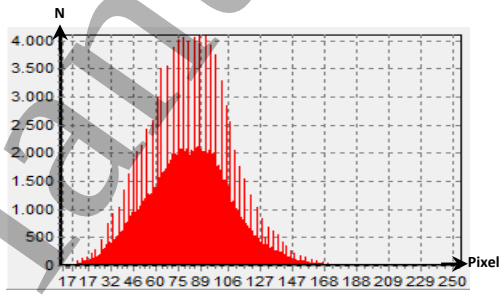

c) Fractal Dimension

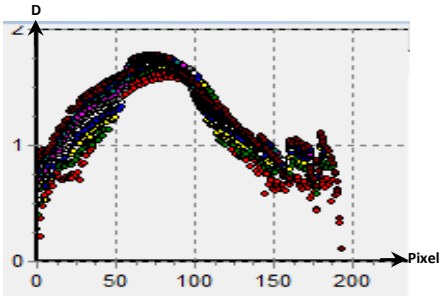

Figure 16. Multifractal analysis for the vorticity structure in the case of a neutral ABL slab. The PDF of vorticity values is almost Gaussian, while the multifractal spectra c) shows the high vorticity peaks due to the propagation of vorticity waves. Vorticity_neutral_horbw

This equation may be used to interpret the different terms that modify the intermittency of the flow. For selected times and ABL flows, we have used multifractal analysis.

The ImaCalc program was used to study the fractal parameter, structure function for different geophysical objects [33-35]. We calculated the maximum value of fractal dimension D selected among all of the velocity intensity and

vorticity modules which is a good indicator of flow's complexity. The data of evolution of D(t) in the middle section of the domain along the main axis were also calculated.

The same approach was used in the single wind turbine wake study [36]. The structure functions, scaling exponents and intermittency in the wake of two wind turbines were studied in the paper [37].

In this section, the analysis of different maps of velocity or vorticity to estimate and compare the fractal dimension, for image between Figure 16 to Figure 18, using the ImaCalc software the latter a) represent the image study in 2 directions, b) represent the histogram of the image between 0 to 256 gray scale, and c) is the fractal dimension graphic of each case.

a) Image of the velocity field

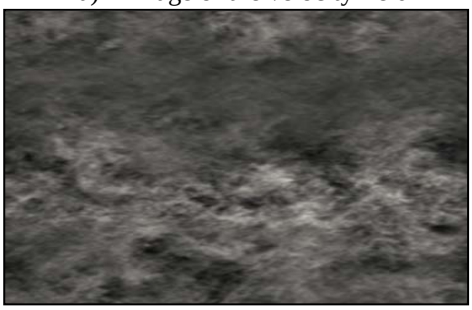

b) Histogram of the image

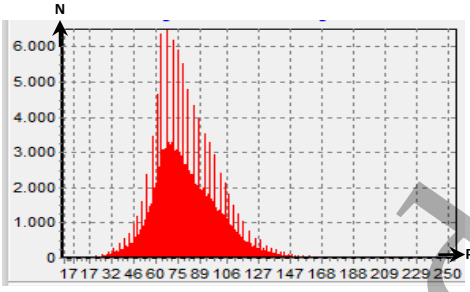

c) Fractal Dimension

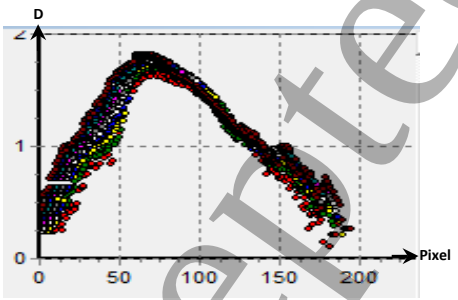

Figure 17. Analysis of the Stably stratified velocity structure (Umag_stable_horbw0).

The results of data processing by means of the ImaCalc program for velocity and vorticity fields, calculation of the fractal dimension, multifractal spectra result for the neutral case are shown in Figures 16 to Figure 18.

In Figures 16 and 17, the maps of velocity and vorticity show a histogram between values of 30 to 168 pixels in gray scale and values of fractal dimension between 0.5 to 1.5. and the analysis of the maps of vorticity in the same area of study (Figure 17), with similar shapes of the histogram but the graphic fractal dimension presents a little difference (more parabolic), but the values of a fractal dimension are in the same range presented in Figure 16 and 17.

a) Image of vorticity field

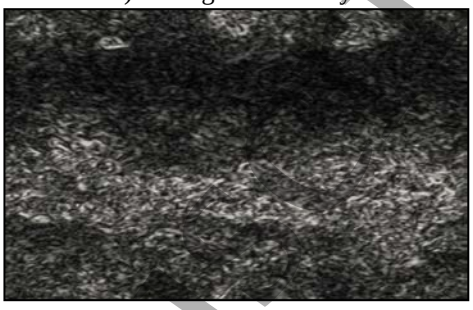

b) Histogram of the image

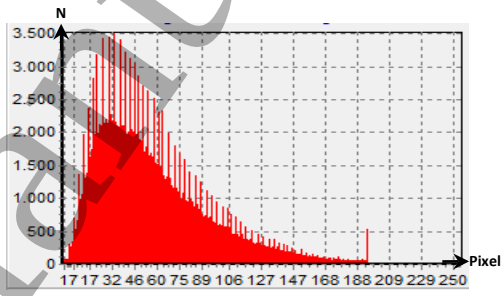

c) Fractal Dimension

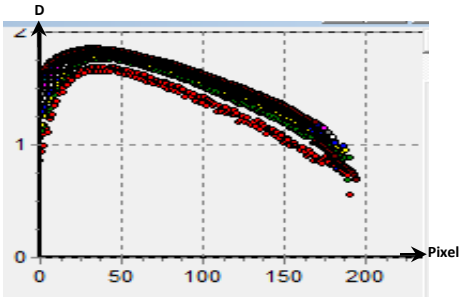

Figure 18. Vorticity_stable_horbw0. c) shows, in this case, the absence of peaks due to the lack of vorticity waves.

The shape of an equilibrium turbulence multifractal spectra is parabolic. The skewness is also related to the velocity or vorticity histograms as seen in all figures of ImaCalc. The spectra D(x, t) at different times and in different positions along the main axis are also calculated. As a general rule multifractal values of vorticity are smaller, indicating a smoothing of the fields. The intermittency exponent changes for higher values of vorticity up to the maximum of 1.8. The corresponding values of D for the velocity in neutral case vary from 0.1 to 1.9 in Figure 18, where the shape of the spectra of fractal dimension is also parabolic.

The shape of an equilibrium turbulence spectra for the stable case has some changes (Figures 18a), where the vorticity structure in a (z, t) plane for the simulation of the horizontal vorticity in a neutral Atmosphere. The corresponding values of D for the velocity in stable case vary from 0.4 to 1.9. Some reflections of waves at high velocity and vorticity values may be detected due to small peaks within the multifractal spectrum, as seen in figure 17c.

The Fractal dimension of the vorticity maps presented in Figure 18, it graphic present a shape similar to the spectrum of Kolmogorov, it indicates that decay energy of the vortices structure in the ABL has a relation with the fractal dimension. In this case the fractal dimension decay between 1.9 to 0.9.

Additional analysis of the fractal dimension with a ABL with a stratification area, in this case, was more difficult to study, because is possible to visualize that in the histogram of the ABL, is possible to see a non-uniform histogram, and for instant the fractal dimension present in Figure 20, the shape is thick with values between 1 to 1.8.

9. Conclusions

We analyse the Atmospheric Boundary Layer (ABL) structure, using a Large-Eddy Simulation (LES) in order to improve pollution topology and diffusion [1].

Many processes are highly intermittent with spiky measures and non-uniformities in Weibull PDF's. For example, distribution of turbulent kinetic energy dissipation rates are intermittent and cannot be described by typical moment methods. Therefore, a multifractal analysis is required. Multifractal dimension was applied to the results of LES and One Eddy Equation turbulence model for neutral and stable ABL in OpenFOAM. The filtered incompressible Navier-Stokes equations within a rotating frame of reference were used to perform additional simulations. Boussinesq approximation for buoyancy was included with an explicit additional term [2].

The size of the numerical domain was 3000x1020x3000 m, meshes with 150x51x150, 300x102x300 cells were used. The initial conditions for the stable case were: wind speed U0=8 m/s with direction 2700, the height at which mean wind (U0) was maximum is 100 m; initial potential temperature at bottom 300 K, at top 305 K; the height of the middle of the inversion was 750 m; the initial turbulent kinetic energy 0.1 m2 /s2; the potential temperature gradient above the inversion was 0.003 K/m. The Prandtl number is 0.7, the turbulent Prandtl (or Schmidt) number 0.33, molecular viscosity 1.0E-5 m2/s, and latitude of the Earth 41.30 degree.

Fractal objects are irregular in shape but their irregularity is similar across many scales, and we applied for these advances in fluid visualization as SFIV to investigate different scale to scale properties of flow through iterative box-counting algorithms for different values of velocity and vorticity

The number of different simulations to be compared is huge but the Multifractal techniques we used to evaluate intermittency and structure functions in the few clear cases of discrimination ability. One such case is only comparing the global Richardson number with the maximum Fractal dimension, the general law is parabolic. Low Richardson numbers indicate high fractal dimensions and vice versa.

Maximum fractal dimension D(RI) as a function of Richardson's number, selected among velocity and vorticity modules which is a good indicator of the flow's complexity.

A methodology has been established for simulation of neutral and stable atmospheric boundary layers and POD analysis. As a result of calculation, it was obtained that 4 first mode contained 95% of the general energy. Q-criterion, lambda2 criterions can be applied for the definition of vorticity and vortex structure dynamics in ABL. The calculations for ABL cases were run on a high-performance cluster as a part of UniHUB web-laboratory on 12-128 cores.

Further, it is planned to provide researches of dynamics for vortex structures taking into account use of standard Smagorinsky model, the model for one differential equation for sub grid kinetic energy and influence of change for the value of heat flux at the Earth's surface.

The analysis of fractal dimension was done using the ImaCalc program. The corresponding values of D for the velocity in neutral case vary from 0.9 to 1.9. Normally the shape of the fractal dimension is parabolic.

The shape of an equilibrium turbulence spectra for the stable case has some changes (Figures 16, 18). The corresponding values of D for the velocity in stable case vary from 0.9 to 1.9.

The fractal dimension of the vorticity maps, considering the effect of the turbulence, intermittency and vortices structure of the ABL, vortex scale are similar to the Kolmogorov spectrum.

Acknowledgements

Authors wishing to acknowledge financial support from RFBR (Grant No. 17-07-01391).

Additional support for travel by European Research Community on Flow, Turbulence and Combustion (ERCOFTAC) and the Pan European Laboratory on Non-Homogeneous Turbulence (PELNoT).

References

[1] Deardorff J W 1970 A three-dimensional numerical investigation of the idealized planetary boundary layer. Geophys Fluid Dyn. 1(3–4) 377–410.

[2] Deardorff J W 1972 Numerical investigations of neutral and unstable planetary boundary layers. J. Atmos Sci. 29 91–115.

[3] Moeng C H A 1984 large-eddy simulation model for the study of planetary boundary layer turbulence. J. Atmos. Sci. 41 2052–2062.

[4] Moeng C H, Sullivan P P 1994 A comparison of shear- and buoyancy-driven planetary boundary layer flows. J. Atmos. Sci. 51 999–1022.

[5] Calaf M, Meneveau C, Meyers J 2010 Large eddy simulations of fully developed wind-turbine array boundary layers. Phys. Fluids. 22 015110.

[6] Churchfield M J, Lee S, Michalakes J, Moriarty P J 2012 A numerical study of the effects of atmospheric and wake turbulence on wind turbine dynamics. Journal of Turbulence. 13, No. 14 1–32.

[7] VerHulst C, Meneveau C 2014 Large eddy simulation study of the kinetic energy entrainment by energetic turbulent flow structures in large wind farms. Phys. Fluids. 26.

[8] Hunt J C R, Morrison J F 2000 Eddy structure in turbulent boundary layers. Eur. J. Mech. B - Fluids. 19 673–694.

[9] Adrian R J 2007 Hairpin vortex organization in wall turbulence. Phys Fluids. 19(4) 041301.

[10] Esau I N 2003 The Coriolis effect on coherent structures in planetary boundary layers. Journal of Turbulence. 4. 017.

[11] Zilitinkevich S S, Hunt J C R., Grachev A A Esau I N, et al. 2006 The influence of large convective eddies on the surface layer turbulence. Quart. J. Roy. Meteorol. Soc. 132 1423-1456.

[12] Huang J, Cassiani M, Albertson J D 2009 Analysis of coherent structures within the atmospheric boundary layer, Boundary-Layer Meteorology. 131 147–171.

[13] Shah S, Bou-Zeid E 2014 Very-Large-Scale Motions in the Atmospheric Boundary Layer Educed by Snapshot Proper Orthogonal Decomposition, Boundary-Layer Meteorology. 153, issue 3 355-387.

[14] Sagaut P 2002 Large eddy simulation for incompressible flows: an introduction. Springer, Berlin, p 426.

[15] Germano M, Piomelli U, Moin P, Cabot W H. 1991 A dynamic subgrid-scale eddy viscosity model. Phys. Fluids 3 1760–1765.

[16] Meneveau C, Lund T S, Cabot W H. 1996 A Lagrangian dynamic subgrid-scale model of turbulence. J Fluid. Mech 319 353–385.

[17] Oliveira P J, Issa R I 2001 An improved PISO algorithm for the computation of buoyancy-driven flows. Numerical Heat Transfer, Part B 40 473.

[18] Schumann U 1975 Subgrid-Scale Model for Finite-Difference Simulations of Turbulent Flow in Plane Channels and Annuli. Journal of Computational Physics, 18 76–404.

[19] Churchfield M J, Moriarty P J, Vijayakumar G, Brasseur J G 2010 Wind Energy-Related Atmospheric Boundary Layer Large-Eddy Simulation Using OpenFOAM. Conference Paper NREL/CP-500-48905 August 2010. 1-26.

[20] Berkooz G, Holmes P, Lumley J 1993 The proper orthogonal decomposition in the analysis of turbulent flows, Annual review of fluid mechanics, 25, no. 1 539–575.

[21] Sirovich L 1987 Turbulence and the dynamics of coherent structures, Part I: coherent structures. Q. Appl. Math. XLV 561–571.

[22] Beare R J, MacVean M K et al. 2006 An intercomparison of large-eddy simulations of the stable boundary layer. Boundary-Layer Meteorology. 118 247-272.

[23] The GABLS stable boundary layer LES intercomparison homepage, 2006, http://gabls.metoffice.com/index.html.

[24] Mandelbrot J B 1993 The Fractal Geometry of Nature, Freeman, New York. 468 p.

[25] Redondo J M 2002 Mixing efficiencies of different kinds of turbulent processes and instabilities, Applications to the environment. in Turbulent mixing in geophysical flows. Eds. Linden P.F. and Redondo J.M. 131-157.

[26] Kolmogorov A N 1941 The local structure of turbulence in Incompressible viscous fluid at very large Reynolds numbers. C. R. Acad. Sci. URSS 30:301.

[27] Kolmogorov A N 1962 A refinement of previous hypotheses concerning the local structure of turbulence in a viscous incompressible fluid at high Reynolds number, J. Fluid Mech. 13, 82-85.

[28] Ben-Mahjoub, O 2000 Non-local dynamics and intermittency in non-homogeneous flows. Tesis Doctoral. The Technical University of Catalonia.

[29] Ben-Mahjoub O, Babiano A and Redondo J M 1998 Structure Functions in Complex Flows. Applied Scientific Research. 59: 299-313.

[30] Frisch U 1995 Turbulence. The legacy of A. N. Kolmogorov. Cambridge: Cambridge University Press.

[31] Mandelbrot B. B. 1975 On the geometry of homogeneous turbulence, with stress in the fractal dimension of the iso-surfaces of scalars. Journal of Fluid Mechanics. 72(03): 401-416.

[32] Sreenivasan K R 1991 Fractal and Multifractals in Fluid Turbulence, Annu. Rev. Fluid Mech. 23, 539-600.

[33] Vindel JM, Yage C, Redondo J. M 2008 Structure function analysis and intermittency in the atmospheric boundary layer. Nonlinear Processes Geophys., vol. 15. pp.915-929.

[34] Ciuchi F, Sorriso-Valvo L, Mazzulla A, Redondo JM 2009 Fractal aggregates evolution of methyl red in the liquid crystal," The European Physical Journal E, vol. 29(2), pp.139-47, 2009.

[35] Tarquis A. M., Platonov A, Matulka A, Grau J, Sekula E, Diez M, and Redondo JM 2014 Application of multifractal analysis to the study of SAR features and oil spills on the ocean surface, Nonlin. Processes Geophys. 21, 439-450.

[36] Strijhak S, Redondo JM, Tellez J 2017 Multifractal analysis of a wake for a single wind turbine, Topical Problems of Fluid Mechanics 2017: Proceedings. – Prague, pp. 275-284.

[37] Kryuchkova A, Tellez-Alvarez J, Strijhak S, Redondo JM 2017, Assessment of Turbulent Wake Behind Two Wind Turbines Using Multi-Fractal Analysis. Ivannikov ISPRAS Open Conference (ISPRAS), 110-116.

[38] Tijera M., Cano J. L., Cano D., Bolster D. and Redondo J.M.: Filtered deterministic waves and analysis of the fractal dimension of the components of the wind velocity. Il Nuovo Cimento C. Geophysics and Space Physics, 31, 653 - 667. (2008).